

The solar oxygen crisis: Probably not the last word

H. Socas-Navarro

High Altitude Observatory, NCAR¹, 3080 Center Green Dr, Boulder, CO 80301, USA

navarro@ucar.edu

A. A. Norton

National Solar Observatory, 950 N. Cherry Ave., Tucson, AZ 85719, USA

norton@nso.edu

ABSTRACT

In this work we present support for recent claims that advocate a downward revision of the solar oxygen abundance. Our analysis employs spatially-resolved spectro-polarimetric observations including the Fe I lines at 6302 Å and the O I infrared triplet around 7774 Å in the quiet Sun. We used the Fe I lines to reconstruct the three-dimensional thermal and magnetic structure of the atmosphere. The simultaneous O I observations were then employed to determine the abundance of oxygen at each pixel, using both LTE and non-LTE (NLTE) approaches to the radiative transfer. In this manner, we obtain values of $\log \epsilon_{\text{O}}=8.63$ (NLTE) and 8.93 (LTE) dex. We find an unsettling fluctuation of the oxygen abundance over the field of view. This is likely an artifact indicating that, even with this relatively refined strategy, important physical ingredients are still missing in the picture. By examining the spatial distribution of the abundance, we estimate realistic confidence limits of approximately 0.1 dex.

Subject headings: Sun: abundances – Sun: granulation – stars: abundances – stars: atmospheres

Oxygen is the third most abundant chemical element in the universe. Its abundance in the solar atmosphere has been traditionally accepted to be approximately $\log \epsilon_{\text{O}}=8.93$ (Anders & Grevesse 1989), with only minor corrections until recently (e.g., $\log \epsilon_{\text{O}}=8.83$ by Grevesse & Sauval 1998). These determinations are based on the use of one-dimensional (1D) semiempirical models (such as those of Holweger & Mueller 1974; Gingerich et al. 1971; Vernazza et al. 1981) to fit spectral features produced by oxygen atoms and molecules. The most common abundance indicators are: the forbidden [O I] line at 6300 Å (e.g., Lambert 1978; Allende Prieto et al. 2001), the infrared (IR) triplet around 7774 Å (e.g., Asplund et al. 2004; Shchukina et al. 2005), as well as molecular bands of OH (e.g., Asplund et al.

2004; Meléndez 2004) and CO (e.g., Ayres et al. 2006; Scott et al. 2006).

Controversy was sparked when Asplund et al. (2004) applied a new hydrodynamic simulation of the solar granulation to the determination of the oxygen abundance, resulting in a considerably lower value ² of $\log \epsilon_{\text{O}}=8.66$. The new value presents some advantages, such as better agreement between various indicators (IR triplet, [O I] and OH vibrational and roto-vibrational bands). It also leads to a better fit of the solar chemical composition within its galactic environment (see, e.g., Sofia & Meyer 2001 and references therein). On the down side, the traditional composition had led to a truly remarkable agreement between the sound speed predicted by solar interior mod-

¹The National Center for Atmospheric Research (NCAR) is sponsored by the National Science Foundation.

² Although a low abundance had been previously derived on Allende Prieto et al. (2001) based on the analysis of the forbidden line at 6300 Å.

els and the helioseismical inversions. A revision of the oxygen abundance, along with the cascading effects on nitrogen, carbon and neon, would require a thorough reworking of that comparison and some recent work (Delahaye & Pinsonneault 2006; Basu et al. 2007) already argues for its incompatibility. The far-reaching implications of the proposed change (notice that it represents a factor of two in the actual number densities) has prompted Ayres et al. (2006) to label this problem as *the solar oxygen crisis*.

In their work, Ayres et al. (2006) derive a semiempirical 1D model of the average thermal stratification and use it to obtain the oxygen abundance from observed CO bands. This approach led them to recommend a rather high value of $\log \epsilon_{\text{O}}=8.85$, consistent with the *traditional* determinations. While discussing the discrepancy with the Asplund et al. (2004) results, they correctly point out that a 3D theoretical simulation is not necessarily superior to a 1D semiempirical model when used for the diagnostics of observations. They both have advantages and drawbacks.

The approach taken here tries to capture the best elements of both worlds, by building a semiempirical 3D model of the solar photosphere. The data set was acquired on 2006 Oct 27 with the Spectro-Polarimeter for Infrared and Optical Regions (SPINOR, Socas-Navarro et al. 2006). It consists of a high-resolution (0.7") spectropolarimetric scan of a quiet Sun region including two Fe I lines at 6302 Å and the oxygen infrared triplet at 7774 Å. The Fe I lines have been used to build the semiempirical 3D model, while the O I triplet is employed for the abundance determination. Since both sets of lines have been observed simultaneously, there is full consistency between the data employed to construct the model and to derive the abundances.

Our 3D model has been obtained from the inversion of the well-known Fe I lines at 6301.5 (for which the oscillator strength has been measured in the laboratory, Bard et al. 1991) and 6302.5 Å together with the continuum at 7774 Å. For each pixel in the field of view, we derived the vertical stratification of temperature, density, line-of-sight velocity and longitudinal magnetic field (details on the Fe I observations and the inversion will be provided elsewhere). We impose the condition that the average observed quiet Sun continuum inten-

sity matches that of the Harvard Smithsonian Reference Atmosphere (HSRA, see Gingerich et al. 1971). Although microturbulence is permitted as a free parameter, the inversion code always retrieved very small values ($\sim 100 \text{ m s}^{-1}$). The model is publicly available upon request from the authors. The spatial resolution is obviously limited when compared to that of the Asplund et al. simulations, but it is sufficient to resolve the granulation. Moreover, those pixels exhibiting significant polarization signal have been treated with a two-component scenario (one for the magnetic concentration and another for the non-magnetic surroundings). Fig 1 shows a composite image of the temperature and the magnetic flux density at the base of the photosphere.

The oxygen abundance was determined independently at each pixel of the map, using the model atmosphere from the Fe I inversion, and accounting for magnetic fields (i.e., considering the Zeeman splitting and solving the Stokes vector transfer equation) where appropriate. Synthetic profiles were computed at intervals of 0.1 dex, and the χ^2 -vs- $\log \epsilon_{\text{O}}$ curve was interpolated to find the minimum with ~ 0.01 dex accuracy (the χ^2 curves obtained are very smooth). For the LTE calculations we used the Stokes synthesis code LILIA (Socas-Navarro 2001), whereas for the non-LTE case we employed the code developed by Socas-Navarro et al. (2000). To alleviate the computational burden we used a 1.5D approach (i.e., neglecting lateral radiative transfer). This approximation is justified by Asplund et al. (2004), who obtained very similar results when comparing 3D and 1.5D syntheses in their simulation. The model atom considered has 13 O I levels plus the continuum, with 18 bound-bound transitions and 13 bound-free (6 of them treated with radiation temperatures). The atomic data are the same as in Carlsson & Judge (1993).

Following the recommendation of Asplund et al. (2004), we neglect excitation and ionization due to inelastic collisions with neutral hydrogen. For the collisional broadening of the lines we employed the formulation of Gray (1976) and tested the influence of the Van der Waals enhancement parameter on the oxygen abundance. For this test we took the spatially-unresolved disk center atlas of Neckel & Labs (1984), inverted the Fe I pair of lines around 6302 Å and used the resulting 1D

model to synthesize the O I IR triplet. Varying the damping enhancement parameter between 0 and 10 had very little influence on the oxygen abundance (~ 0.01 dex). For larger values, the synthetic profiles are too broad to fit the observations. While the enhancement parameter strongly influences the equivalent widths of the lines (because it broadens the wings leaving the cores more or less intact), its effect is less pronounced in our analysis that considers the least-squares fit to the overall profile. In this test with unresolved observations and a 1D model we obtained an oxygen abundance of $\log \epsilon_{\text{O}}=8.66$, which is consistent with the previous 1D NLTE determinations of Asplund et al. (2004) and Shchukina et al. (2005).

Since the O I lines are shallower than the Fe I lines, one would intuitively expect their formation height range to be narrower. In other words, the height range that we need for the synthesis of the O I triplet is contained entirely in the range that we can reconstruct from the Fe I lines. A formal verification of this is presented in Fig 2, which shows the temperature response functions (RFs, see Landi Degl’Innocenti & Landi Degl’Innocenti 1977) of the lines at several wavelengths, from the continuum to the line center. RFs measure how the line profile reacts to atmospheric perturbations at various heights, and therefore provide very valuable information on the sensitivity range of spectral features.

The spatial distribution of $\log \epsilon_{\text{O}}$ obtained with our 3D semiempirical model is shown in Fig 3. In agreement with previous works, we find that the LTE approximation largely overestimates $\log \epsilon_{\text{O}}$ by approximately 0.3 dex (this value is slightly dependent on spatial location). The variation of the inferred $\log \epsilon_{\text{O}}$ over the field of view is due to fluctuations in the solar atmospheric conditions. We can see that the abundance in the pore is considerably higher, reaching values up to 0.3 dex larger than the average, and decreasing gradually as we move away from it. In general, magnetic concentrations exhibit higher abundances. This suggests that previous abundance determinations might be slightly biased by solar (or, more generally, stellar) activity, depending on the phase of the cycle in which the observations were taken. The mean values that we obtained over the entire field of view are $\log \epsilon_{\text{O}}=8.94$ (LTE) and $\log \epsilon_{\text{O}}=8.64$ (NLTE) dex, with standard deviations of 0.08 dex. In the

NLTE case, this is equivalent to a concentration of $\epsilon_{\text{O}}/\epsilon_{\text{H}}$ of $442 (\pm 80) \times 10^{-6}$. If we restrict the analysis to pixels with less than 100 G of flux density, we obtain $\log \epsilon_{\text{O}}=8.93$ (LTE) and $\log \epsilon_{\text{O}}=8.63$ (NLTE).

Obviously, there is no physical reason to expect the actual abundance to exhibit spatial variations in the solar photosphere. We must then conclude that this is an artifact of the analysis, probably due to imperfect modeling especially in the presence of magnetic fields (notice that the granulation pattern is not visible in the abundance images). We stress that the modeling employed here should be more reliable than that in previous works (since it considers 3D geometry, magnetic fields, NLTE and is based on actual observations). Yet, it still falls short of providing a solid, accurate, abundance determination. The uncertainties (~ 0.1 dex) are larger than previously thought (Pinsonneault & Delahaye 2006 have already pointed this out and their error budget is consistent with our figure), and this is also an important point to bear in mind.

The authors are grateful to the NSO staff at Sunspot NM (USA), and particularly the observers, for their support of the SPINOR observations presented here. Thanks are also due to the anonymous referee who helped improve a previous version of the manuscript. HSN also acknowledges partial support from the Spanish Ministerio de Educación y Ciencia through project AYA2004-05792. Some of the processing power used for the calculations in this paper has been generously donated by B. Lites, M. Wiltberger, M. Rempel and J. Borrero.

REFERENCES

- Allende Prieto, C., Lambert, D. L., & Asplund, M. 2001, *ApJ*, 556, L63
- Anders, E., & Grevesse, N. 1989, *Geochim. Cosmochim. Acta*, 53, 197
- Asplund, M., Grevesse, N., Sauval, A. J., Allende Prieto, C., & Kiselman, D. 2004, *A&A*, 417, 751
- Ayres, T. R., Plymate, C., & Keller, C. U. 2006, *ApJS*, 165, 618

- Bard, A., Kock, A., & Kock, M. 1991, *A&A*, 248, 315
- Basu, S., Chaplin, W. J., Elsworth, Y., New, R., Serenelli, A. M., & Verner, G. A. 2007, *ApJ*, 655, 660
- Carlsson, M., & Judge, P. G. 1993, *ApJ*, 402, 344
- Delahaye, F., & Pinsonneault, M. H. 2006, *ApJ*, 649, 529
- Gingerich, O., Noyes, R. W., Kalkofen, W., & Cuny, Y. 1971, *Sol. Phys.*, 18, 347
- Gray, D. F. 1976, *The observation and analysis of stellar photospheres* (Research supported by the National Research Council of Canada. New York, Wiley-Interscience, 1976)
- Grevesse, N., & Sauval, A. J. 1998, *Space Science Reviews*, 85, 161
- Holweger, H., & Mueller, E. A. 1974, *Solar Phys.*, 39, 19
- Lambert, D. L. 1978, *MNRAS*, 182, 249
- Landi Degl’Innocenti, E., & Landi Degl’Innocenti, M. 1977, *A&A*, 56, 111
- Meléndez, J. 2004, *ApJ*, 615, 1042
- Neckel, H., & Labs, D. 1984, *Solar Phys.*, 90, 205
- Pinsonneault, M. H., & Delahaye, F. 2006, *ArXiv Astrophysics e-prints*
- Scott, P. C., Asplund, M., Grevesse, N., & Sauval, A. J. 2006, *A&A*, 456, 675
- Shchukina, N. G., Trujillo Bueno, J., & Asplund, M. 2005, *ApJ*, 618, 939
- Socas-Navarro, H. 2001, in *ASP Conf. Ser. 236: Advanced Solar Polarimetry – Theory, Observation, and Instrumentation*, 487
- Socas-Navarro, H., Elmore, D., Pietarila, A., Darnell, A., Lites, B., & Tomczyk, S. 2006, *Solar Physics*, 235, 55
- Socas-Navarro, H., Trujillo Bueno, J., & Ruiz Cobo, B. 2000, *ApJ*, 530, 977
- Sofia, U. J., & Meyer, D. M. 2001, *ApJ*, 554, L221
- Vernazza, J. E., Avrett, E. H., & Loeser, R. 1981, *ApJS*, 45, 635

This 2-column preprint was prepared with the AAS L^AT_EX macros v5.2.

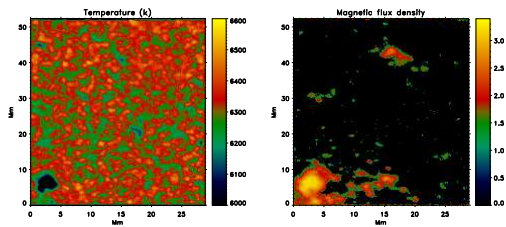


Fig. 1.— Maps of the temperature and the magnetic flux density at the base of the photosphere in the 3D model, as derived from the SPINOR data. Left panel: Temperature. In those pixels that exhibit polarization signal, the average temperature inside and outside the magnetic concentration (weighted according to occupation fraction) is depicted. The cool feature on the lower left corner is a pore that was used to stabilize the adaptive optics, allowing us to achieve the spatial resolution shown in the image. Right panel: Decimal logarithm of the magnetic flux density in G.

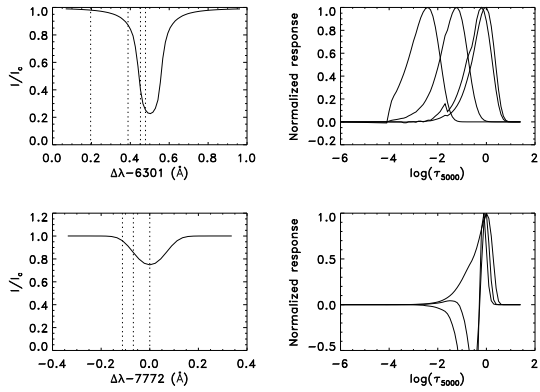


Fig. 2.— Normalized response functions to temperature perturbations, computed in the HSRA quiet Sun model. Left panels: Line profiles of the Fe I 6301 Å (top) and O I 7772 Å (bottom) lines. Right panels: Response of the intensity profile at the wavelengths marked with vertical dotted lines in the left panels, as a function of height where the perturbation occurs. The 7772 Å line is the deepest (darkest core) of the multiplet and therefore spans the broadest height range of the O I triplet. Nevertheless, its formation range is still well within that spanned by the Fe I lines.

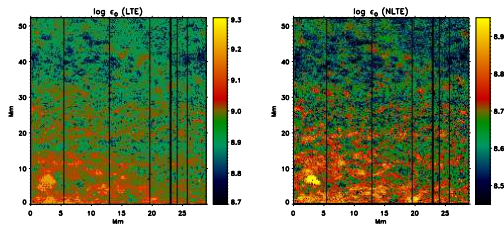


Fig. 3.— Logarithmic oxygen abundance $\log \epsilon_{\text{O}}$ (with the usual convention in Astrophysics that $\log \epsilon_{\text{H}}=12$). Left panel: LTE calculation. Right panel: NLTE calculation. Note that the color scales are different, since the LTE abundances are systematically higher. The vertical lines are missing data due to errors in the detector system that was recording the oxygen data.